Two-Dimensional Time-Domain Inverse Scattering for Quantitative Analysis of Breast Composition

Jessi E. Johnson*, *Member, IEEE*, Takashi Takenaka, *Member, IEEE*, and Toshiyuki Tanaka, *Member, IEEE*

***Abstract*—Forward–backward time-stepping is a unique approach for solving electromagnetic inverse scattering problems in the time domain. In this paper, the technique is applied to a realistic, heterogeneous breast model. The ability to detect a 5-mm diameter malignancy and provide substantial quantitative information about the breast's composition is demonstrated.**

***Index Terms*—Cancer, electromagnetic scattering inverse problems, medical diagnosis, microwave imaging.**

I. Introduction

SHORTCOMINGS in conventional X-ray mammography for breast cancer screening, such as lack of sensitivity (missing up to 15% of tumors) and an unreasonably large amount of false positive readings [1] have led to the search for viable complementary and/or alternative approaches for breast imaging. Although positive clinical results have been shown for imaging modalities such as magnetic resonance imaging (MRI) and ultrasound [1], microwave-based methods have been gaining increasing attention as an advantageous approach to breast cancer detection and analysis [2]. The large contrast in the microwave properties of normal and malignant breast tissue [3], the relatively low-cost of microwave equipment, the use of safe, low-level microwave signals [4], and successful preliminary clinical studies [5] are all reasons suggesting that microwave-based imaging has the potential to make the difficult transition from the laboratory to successful clinical use.

Although a variety of microwave approaches exist for breast cancer detection, arguably the most successful to date have been tomographic, frequency-domain inverse scattering approaches [5] and ultrawideband, radar-based techniques [6], [7]. While the former approach can boast the ability to generate quantitative images in which the internal permittivity (ϵ_r) and conductivity (σ) composition of the breast is reconstructed, the latter has demonstrated the ability to create relatively high-resolution images to detect tumors as small as 2 mm in diameter [3]. In this paper, a technique for breast cancer detection and analysis that combines advantages of these two approaches is presented. In the forward–backward time-stepping (FBTS) technique [8]–[11], broadband microwave signals are utilized to solve the inverse scattering problem in the time-domain. By utilizing a tomographic approach, the FBTS technique has the potential to generate images that provide useful quantitative information about the internal structure of the breast, such as the shape and composition of fibroglandular tissue regions. Additionally, the use of a broadband signal provides a large amount of scattering information about the breast and should allow for stable reconstructions of relatively high-resolution images. Previous investigations of the FBTS technique presented by the authors [8]–[11], as well as similar studies by Fhager *et al.* [12] have demonstrated the efficacy of time-domain inverse scattering for reconstructing simple objects such as cylinders and spheres in a breast-like configuration. An investigation by Winters *et al.* [13] demonstrated that a similar time-domain approach could be utilized to predict average electrical property parameters of the skin and normal tissue regions of a realistic, MRI-derived breast model in 2-D (as a preprocessing technique for radar-based imaging). In this paper, the 2-D FBTS technique described in [9] is extended to a similarly realistic breast model to demonstrate the efficacy of FBTS for tumor detection and quantitative analysis of the breast's internal composition.

Manuscript received February 14, 2007; revised April 5, 2007. *Asterisk indicates corresponding author.* This work was supported by the Japan Society for the Promotion of Science (JSPS) through a Postdoctoral Fellowship for Foreign Researchers.

*J. E. Johnson is with the Department of Electrical and Electronic Engineering, Nagasaki University, Nagasaki 852-8521 Japan (e-mail: johnsonj@ieee.org.

T. Takenaka and T. Tanaka are with the Department of Electrical and Electronic Engineering, Nagasaki University, Nagasaki 852-8521 Japan (e-mail: takenaka@nagasaki-u.ac.jp; t-toshi@nagasaki-u.ac.jp).

Digital Object Identifier 10.1109/TBME.2007.899364

II. Methods

A. FBTS Imaging

In the FBTS technique, errors between measured and simulated microwave scattering measurements are compared in the time-domain and minimized utilizing conjugate gradient optimization. For nonmagnetic inverse scattering problems, the error functional for an assumed set of electrical property parameters p is

$$Q(p) = \int_0^T \sum_{m=1}^{M} \sum_{n=1}^{N} |v_m(p; r_n, t) - \tilde{v}_m(r_n, t)|^2 \, dt \qquad (1)$$

where $v_m(p; r_n, t)$ describes the calculated time-domain electric field at receiving position n due to a pulse radiated by a transmitter m, and $\tilde{v}_m(r_n, t)$ describes the corresponding measured field. Errors between simulation and measurement are summed for multiple transmitter/receiver combinations and are integrated over a time period from $t = 0$ to $t = T$. It can be shown that the gradient of this error functional with respect to p can be calculated utilizing a forward finite-difference time-domain (FDTD) computation followed by a corresponding adjoint FDTD computation in which residual received signals $[v_m(p; r_n, t) - \tilde{v}_m(r_n, t)]$ are reversed in time and utilized as sources. Note that, although not utilized in this study, a regularization term can be added to (1) to improve the stability of the

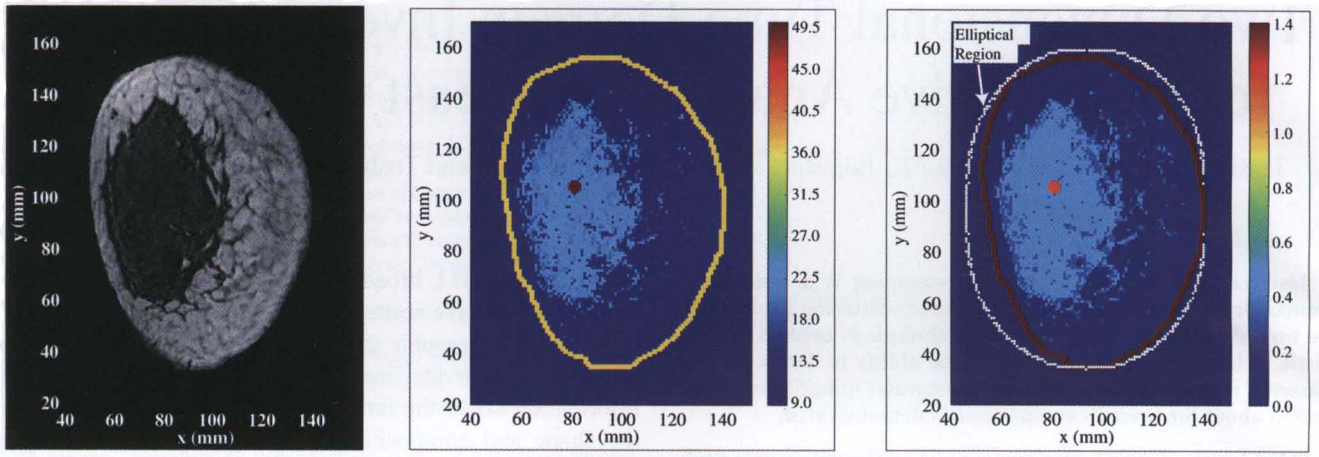

Fig. 1. MRI-derived breast model utilized in this research: (a) original MR image. (b) permittivity model with 2-mm-thick skin layer and 5-mm-diameter tumor in fibroglandular region. (c) corresponding conductivity model.

algorithm, particularly when dealing with noisy measurement data [9]. For more details on the FBTS method, please refer to [8]–[10].

B. Breast Modeling

A 0.39 mm × 0.39-mm-resolution MR image of the left breast of a volunteer in the prone position was taken at Nagasaki University Hospital, as shown in Fig. 1(a). The histogram of the MR image pixel intensities was utilized to segment the image into distinct fibroglandular and fat tissue regions, with a transition region between the two. First-order Debye model parameters were then mapped to each pixel value using the piecewise-linear mapping procedure described in [14]. Using this method, darker intensity pixels were mapped to $\pm 10\%$ of the nominal Debye parameters for fibroglandular tissue and lighter pixels mapped to $\pm 10\%$ of the nominal parameters for fat tissue. A simple linear map was then utilized to span between these two regions. The model was resized to a resolution of 1 mm × 1 mm, and a 2-mm-thick skin layer was added. A 5-mm-diameter tumor was then added to the model, inside the fibroglandular region. Finally, since the following analysis was conducted assuming dispersionless media, all of the Debye parameters for the model were evaluated at a frequency $f_c = 2$ GHz. This procedure resulted in the realistic heterogeneous model of the permittivity and conductivity of the breast, as shown in Fig. 1(b) and (c). The values of the nominal Debye parameters for the various tissue types were taken from [14] and the resulting permittivity and conductivity values at 2 GHz are as follows: fibroglandular $\epsilon_r = 21.45$ $\sigma = 0.46$; fat $\epsilon_r = 9.98$ $\sigma = 0.18$; skin $\epsilon_r = 36.73$ $\sigma = 1.43$; tumor $\epsilon_r = 53.62$ $\sigma = 1.19$.

C. Reconstructions

Two-dimensional FDTD (TM_z mode) simulation was utilized to characterize the microwave scattering of the breast model at 16 points encircling the breast. Each of the 16 points were used sequentially as a transmitter (represented by a simple line source in the FDTD simulation), with the electric field being sampled at the remaining 15 points. This set of scattering calculations (representing 240 transmitter/receiver combinations) formed a set of numerical "measured" data that was utilized for the $\tilde{v}_m(r_n, t)$ term of (1). The grid size for the FDTD simulation was 1 mm × 1 mm, and the excitation signal was a sinusoidally modulated Gaussian pulse with a center frequency $f_c = 2$ GHz and a 1.3 GHz bandwidth. This frequency range was determined in previous studies [9] to be optimum for simple reconstructions of a breast-like configuration. Although it is possible to use higher frequency signals ($f_c = 4$ GHz or larger) for obtaining higher resolution images of smaller tumors [12], this leads to a less stable inverse problem that requires multi-frequency techniques, as discussed in [9] and [10]. For this preliminary investigation, it was assumed that the breast was immersed in a lossless ($\sigma = 0.0$) coupling liquid with a permittivity that roughly matches breast fat ($\epsilon_r = 9.0$); however, a variety of coupling liquids have been shown to give similar results in other studies [15].

After forming the set of numerical measured data, the FBTS technique was utilized to reconstruct the breast model. Reconstructions were conducted utilizing a 1 mm × 1 mm FDTD grid and the optimization was carried out for 250 iterations. The efficacy of the FBTS algorithm was assessed by conducting several reconstructions and assuming different, increasingly accurate *a priori* estimates for the properties of the breast. These estimates are described as follows:

Estimate A: The reconstruction region has a shape that estimates the surface of the breast as an ellipse, as shown in Fig. 1(c). The initial ϵ_r and σ values in this entire region are set equal to the coupling liquid ($\epsilon_r = 9.0$ and $\sigma = 0.0$).

Estimate B: The reconstruction region matches the shape of the breast exactly. The initial ϵ_r and σ values are set equal to the coupling liquid in the entire region.

Estimate C: The reconstruction region matches the shape of the breast. In this case (only) it is also assumed that the location of the skin region has been predicted and assigned initial ϵ_r and σ values equal to $+10\%$ of the actual values. ϵ_r and σ in the remaining "normal" breast region are set equal to the coupling liquid.

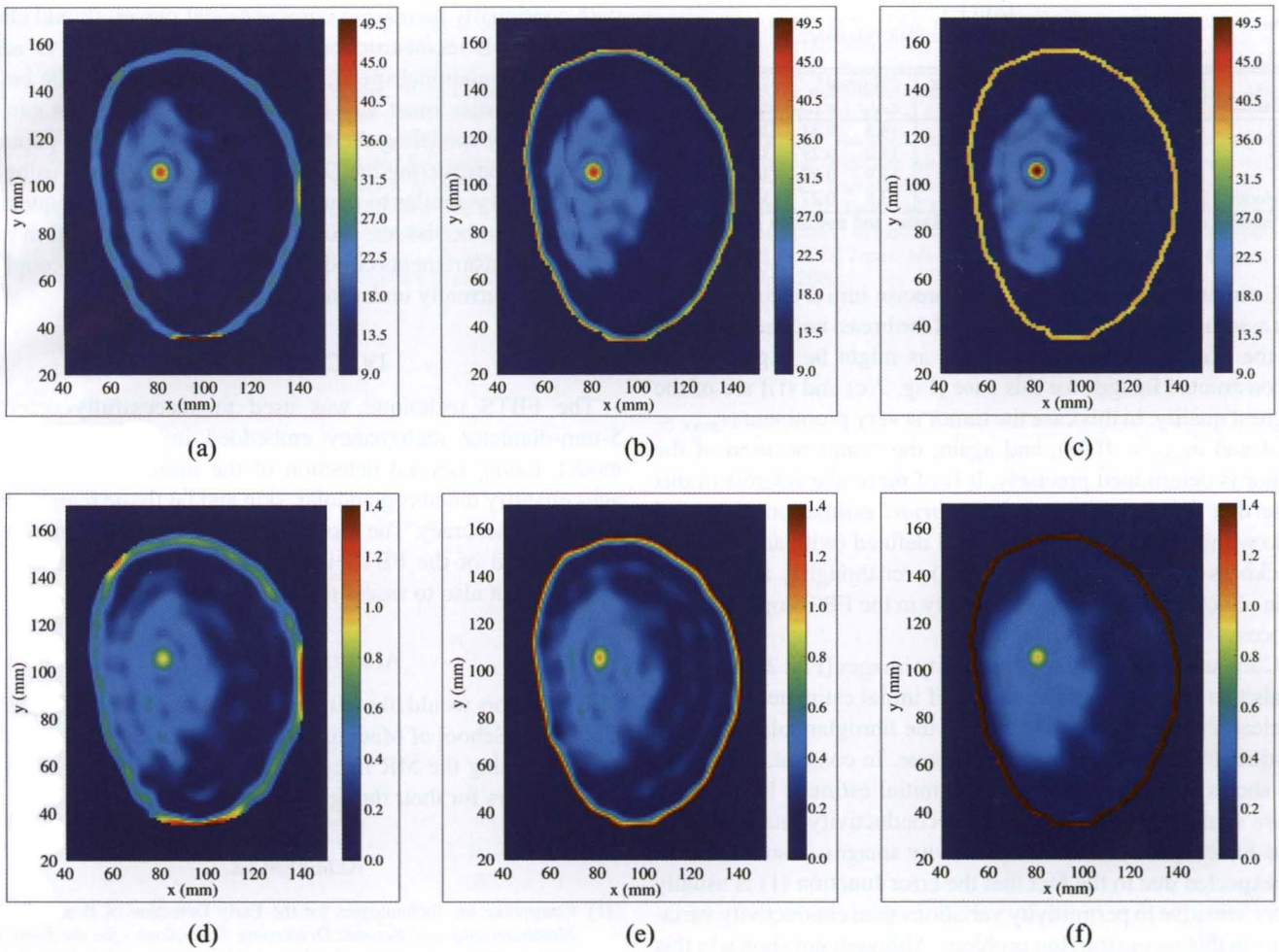

Fig. 2. FBTS images of breast model with 5-mm lesion in the fibroglandular region. Parts (a)–(c) show permittivity reconstructions for initial estimates A, B, and C, respectively. Parts (d)–(f) show the corresponding conductivity reconstructions.

Although estimates B and C assume that a fairly large amount of *a priori* information can be obtained about the breast, microwave-based techniques for breast surface identification (BSID) [16], skin thickness prediction [17], and the aforementioned approach for estimating average tissue properties [13] should make it feasible in the future to form such accurate, patient-specific initial estimates for FBTS imaging.

III. Results And Discussion

Fig. 2 shows the reconstructed images utilizing the FBTS technique and compares the results for the three initial estimates A–C. Observing the images for which the elliptical reconstruction region was utilized [Estimate A, shown in Fig. 2(a) and (d)], it is clear that both the permittivity and conductivity reconstructions distinctly show the presence of the lesion in the breast. The center position of the tumor is $x = 80$ mm, $y = 105$ mm for both images, corresponding exactly to the actual tumor position. The peak values for the tumor are $\epsilon_{\max} = 43.6$ and $\sigma_{\max} = 0.92$, which are significantly lower than the actual values of $\epsilon_{\max} = 53.6$ and $\sigma_{\max} = 1.19$. In comparing Fig. 2(a) and (d) it is evident that the permittivity image is more accurate. This is particularly noticeable in the skin region, with the reconstructed skin layer being wider and more blurry in the conductivity image. The estimated skin thickness, calculated using the full-width half-maximum permittivity (conductivity) span over several 1-D lines tracing through the skin region, is 4.6 mm for the permittivity image and 5.3 mm for the conductivity image. The fibroglandular region is also more well defined in the permittivity image, which is evident by the area on the left side of the image where a thin strip of fat tissue exists between the skin and the fibroglandular region. For the conductivity reconstruction, this strip of fat tissue is indistinguishable from the fibroglandular tissue.

Fig. 2(b) and (e) shows the permittivity and conductivity images when the reconstruction region is constrained to the actual position of the breast (Estimate B). In this case, the center position of the tumor is also detected exactly and the tumor is more prominent ($\epsilon_{\max} = 45.7$ and $\sigma_{\max} = 1.01$) than for Estimate A. Comparison of Fig. 2(a) and (b) demonstrates that either initial estimate results in similar reconstructed permittivity image quality. However, it is clear that the skin region is much more well defined when using Estimate B, with an estimated thickness of 2.4 mm using the ϵ_r image (and 2.1 mm using the σ image). Additionally, when comparing the conductivity images [Fig. 2(d) and (e)], it can be seen that Estimate B results in a better reconstruction of the fibroglandular region.

TABLE I
CHARACTERISTICS OF RECONSTRUCTED IMAGES

Estimate	Tumor		Fibroglandular		Normal*		Skin	
	ϵ_{max}	σ_{max}	ϵ_{avg}	σ_{avg}	ϵ_{avg}	σ_{avg}	ϵ_{avg}	σ_{avg}
A	43.6	0.92	20.1	0.42	14.5	0.31	24.6	0.68
B	45.7	1.01	20.1	0.43	14.2	0.29	32.6	1.21
C	51.4	0.98	20.2	0.43	13.9	0.27	36.6	1.47
Model	53.6	1.19	21.6	0.46	13.8	0.27	36.7	1.43

*normal region includes the fat, fibroglandular, and transition regions

Estimate C represents the most precise initial estimate, with the assumption that both the shape of the breast and the thickness of the skin can be detected. Thus, as might be expected, the reconstructed images for this case [Fig. 2(c) and (f)] are of the highest quality. In this case the tumor is very prominent ($\epsilon_{\max} = 51.4$ and $\sigma_{\max} = 0.98$), and again, the center position of the tumor is determined precisely. It is of particular interest in this case that the skin region, after *a priori* estimation of ϵ_r and σ to within 10%, remains very well defined (with an estimated thickness of 2.3 mm for both images) even though ϵ_r and σ in the skin region are allowed to vary freely in the FBTS optimization process.

Comparison of all three permittivity images [Fig. 2(a)–(c)] reveals that regardless of the choice of initial estimate, the tumor is clearly detected and the shape of the fibroglandular region is distinct from the surrounding fat tissue. In contrast, Fig. 2(d)–(f) shows that the accuracy of the initial estimate has a much more significant influence over the conductivity image quality. The lower quality of the conductivity images is somewhat to be expected due to the fact that the error function (1) is usually more sensitive to permittivity variations than conductivity variations in this reconstruction problem. Although not shown in this paper, this difference in sensitivity is evident when comparing the effects of changes in the shape of scattered waveforms for variations in conductivity with variations in permittivity.

In order to further assess the quality of the images in Fig. 2, the average ϵ_r and σ values of the fibroglandular, skin, and normal tissue regions (determined using the proper sets of pixels as identified during the breast modeling step) were calculated (see Table I). Observing these results, it is striking how closely the average values in the different tissue regions are reproduced, particularly for the most precise initial estimate (C). However, even for the least precise estimate (A), the average ϵ_r values of the fibroglandular and normal tissue regions are predicted to within 7% of the actual values. Similarly, the σ values in this case are predicted to within 14%. Thus, although the skin region reconstruction quality is poor for Estimate A, the internal composition of the breast is still reconstructed with reasonable accuracy.

Finally, there are some practical issues in the future development of the FBTS technique that warrant some discussion. In this 2-D study, imaging times were reasonable (2.6 min/iteration on a personal computer (PC) with an AMD Athalon 4000+ 64-bit processor and 4 GB RAM); however, 3D reconstructions will be significantly slower. Fortunately it is possible to implement the FBTS algorithm in a parallel process, with gradients for each transmitter calculated individually on separate processors. Techniques such as this, combined with the availability of PCs with continually increasing computational power, should allow for future 3-D reconstructions with reasonable speed. In addition to computational speed, frequency dispersion of the breast tissue properties must also be considered. Dispersion can be addressed by modeling the breast tissues with Debye parameters and reconstructing the Debye parameters directly, using an approach very similar to that described in [13]. Techniques for overcoming other issues, such as integrating the algorithm with practical measurements conducted in a tank filled with coupling liquid, are currently under investigation.

IV. CONCLUSION

The FBTS technique was used to successfully detect a 5-mm-diameter malignancy embedded in a realistic breast model. Going beyond detection of the tumor, the FBTS images quantify the fibroglandular, skin and fat tissue regions with significant accuracy. The results from this research demonstrate the potential of the FBTS approach to be useful not just for detection but also to assess the breast's internal composition.

ACKNOWLEDGMENT

The authors would like to thank Dr. I. Isomoto of the Nagasaki University School of Medicine for his assistance with acquiring and processing the MR images. They would also like to thank the reviewers for their thoughtful suggestions.

REFERENCES

[1] Committee on Technologies for the Early Detection of Breast Cancer, *Mammography and Beyond: Developing Technologies for the Early Detection of Breast Cancer*, S. Nass, I. Henderson, and J. Lashof Eds. Washington, DC: National Cancer Policy Board, Institute of Medicine, and Commission on Life Studies, National Research Council, 2001.

[2] E. Fear, S. Hagness, P. Meaney, M. Okoniewski, and M. Stuchly, "Enhancing breast tumor detection with near-field imaging," *IEEE Microw. Mag.*, vol. 3, no. 1, pp. 48–56, Mar. 2002.

[3] X. Li, E. Bond, B. Van Veen, and S. Hagness, "An overview of ultra-wideband microwave imaging via space–time beamforming for early-stage breast-cancer detection," *IEEE Antennas Propag. Mag.*, vol. 47, no. 1, pp. 19–34, Feb. 2005.

[4] J. Johnson and T. Takenaka, "Preliminary assessment of electromagnetic absorption in the breast for cylindrical microwave breast cancer detection systems," in *Proc. Progress Electromagn. Res. Symp.*, Tokyo, Japan, 2006, pp. 256–260.

[5] P. Meaney, M. Fanning, D. Li, S. Poplack, and K. Paulsen, "A clinical prototype for active microwave imaging of the breast," *IEEE Trans. Microw. Theory Tech.*, vol. 48, no. 11, pp. 1841–1853, Nov. 2000.

[6] E. Fear, X. Li, S. Hagness, and M. Stuchly, "Confocal microwave imaging for breast cancer detection: Localization of tumors in three dimensions," *IEEE Trans. Biomed. Eng.*, vol. 49, no. 8, pp. 812–822, Aug. 2002.

[7] X. Li, S. Davis, S. Hagness, D. van der Weide, and B. Van Veen, "Microwave imaging via space–time beamforming: Experimental investigation of tumor detection in multilayer breast phantoms," *IEEE Trans. Microw. Theory Tech.*, vol. 52, no. 8, pp. 1856–1865, Aug. 2004.

[8] T. Takenaka, T. Tanaka, H. Harada, and S. He, "FDTD approach to time-domain inverse scattering problem for stratified lossy media," *Microw. Opt. Technol. Lett.*, vol. 16, no. 5, pp. 292–296, 1997.

[9] T. Takenaka, H. Jia, and T. Tanaka, "Microwave imaging of electrical property distributions by a forward–backward time-stepping method," *J. Electromagn. Waves Appl.*, vol. 14, no. 12, pp. 1609–1626, 2000.

[10] T. Tanaka, N. Kuroki, and T. Takenaka, "Filtered forward–backward time-stepping method applied to reconstruction of dielectric cylinders," *J. Electromagn. Waves Appl.*, vol. 17, no. 2, pp. 253–270, 2003.

[11] J. Johnson, H. Zhou, and T. Takenaka, "Experimental three-dimensional time-domain reconstruction of dielectric objects for breast cancer detection," in *Proc. Mediterr. Microw. Symp.*, 2006, pp. 423–426.

[12] A. Fhager, P. Hashemzadeh, and M. Persson, "Reconstruction quality and spectral content of an electromagnetic time-domain inversion algorithm," *IEEE Trans. Biomed. Eng.*, vol. 53, no. 8, pp. 1594–1604, Aug. 2006.

[13] D. W. Winters, E. J. Bond, B. D. Van Veen, and S. C. Hagness, "Estimation of the frequency-dependent average dielectric properties of breast tissue using a time-domain inverse scattering technique," *IEEE Trans. Antennas Propag.*, vol. 54, no. 11, pp. 3517–3528, Nov. 2006.

[14] M. Converse, E. Bond, B. Veen, and S. Hagness, "A computational study of ultra-wideband versus narrowband microwave hyperthermia for breast cancer treatment," *IEEE Trans. Microw. Theory Tech.*, vol. 54, no. 5, pp. 2169–2180, May 2006.

[15] P. Kosmas, C. Rappaport, and E. Bishop, "Modeling with the FDTD method for microwave breast cancer detection," *IEEE Trans. Microw. Theory Tech.*, vol. 52, no. 8, pp. 1890–1897, Aug. 2004.

[16] D. Winters, B. Van Veen, and S. Hagness, "UWB microwave imaging for breast cancer detection: An algorithm for estimating the breast surface," in *Proc. IEEE Antennas Propag. Soc. Int. Symp.*, Jul. 2006, pp. 267–270.

[17] T. Williams, E. Fear, and D. Westwick, "Tissue sensing adaptive radar for breast cancer detection—Investigations of an improved skin-sensing method," *IEEE Trans. Microw. Theory Tech.*, vol. 54, no. 4, pp. 1308–1314, Jun. 2006.